Vertical isolation of a structure based on different states of seismic performance

Reza Milanchian[1a], Mahmood Hosseini[*2] and Masoud Nekooei[1b]

[1]*Department of Structural Engineering, Science and Research branch, Islamic Azad University, Tehran, Iran*
[2]*Structural Engineering Research Center, International Institute of Earthquake Engineering and Seismology (IIEES), Tehran, Iran*

Abstract. In vertical seismic isolation (VSI), a building is partitioned intentionally by vertical layers into two dynamically different substructures for seismic response reduction. Initially, a 1-story frame was partitioned into two substructures, interconnected by viscous and visco-elastic links, and seismic responses of the original and the vertically isolated structures (VIS) were obtained, considering a large number of stiffness and mass ratios of substructures with respect to the original structure. Color contour graphs were defined for presentation and investigation of large amounts of output results. Dynamic characteristics of the isolated structures were studied by considering the non-classical damping of the system, and then the effects of viscous and visco-elastic link parameters on the modal damping ratios were discussed. On this basis, three states of mass isolation, interactional state, and control mass were differentiated. Response history analyses were performed by Runge-Kutta numerical method. In these analyses, interaction of isolation ratios and link parameters, on response control of VIS was studied and the appropriate ranges for link parameters as well as the optimal ranges for isolation ratios were suggested. Results show that by using the VSI technique, seismic response reduction up to 50% in flexible substructure and even more in stiff substructure is achievable.

Keywords: vertical seismic isolation; non-classical damping; viscous and visco-elastic dampers; Runge-Kutta method; response history analyses

1. Introduction

The seismic design philosophy of new structures in current building codes is based on the system ductility. In conventional design procedures, energy absorption capacity is provided in certain elements of the structure. Some structural elements are designed and detailed with large plastic deformation capacities. Even if properly designed, damage and large deformations in the structure's elements are inevitable, particularly in case of large earthquakes. Hence, there is an increasing need for more innovative and efficient lateral displacement control strategies. Instead of ductility, innovative approaches in the seismic design of structures are based on structural interaction, the use of flexibility and energy dissipation capacities of the buildings to receive less earthquake input force and energy. In this manner, the energy is dissipated with lower damage and deformations in the structural members.

The root of the vertical seismic isolation (VSI) idea is similar to that of coupled buildings or adjacent structures, which was first introduced by Klein, Todaro *et al.* (1972)

for reducing the wind-induced vibration in large structures. Coupled buildings idea was further developed by Xu *et al.* (1999) as also Zhang and Xu (1999) employing linking dampers. They determined the optimal values of connecting links by extensive parametric studies for achieving the maximum modal damping ratio or the maximum response reduction of adjacent buildings. Zhang and Xu (2000) also studied coupled buildings linked by Maxwell model-defined fluid dampers. They used complex modal superposition method to determine dynamic characteristics of linked adjacent buildings and then (Zhu and Xu 2005) worked on optimizing the parameters of those fluid dampers by the analytical formulas which were derived using the principle of minimizing the averaged vibration energy of adjacent structures under a white-noise ground excitation. Patel and Jangid (2010) utilized numerical approaches to determine the optimal parameters for connection elements in two adjacent buildings. Zhu *et al.* (2011) studied on optimum connecting visco-elastic and viscous dampers to reduce the seismic responses of parallel structures. They selected two optimization criteria to minimize the vibration energy of the two adjacent structures. Richardson *et al.* (2013) discussed the merit of generating sufficient control forces at low frequencies, a property that is necessary for minimizing the displacement response of high-rise structures, and derived closed-form equations for solving the vibration control problem of connecting two adjacent structures.

Numerous studies have been performed to investigate strategies for reducing the response of adjacent structures based on active and semi-active control. The effectiveness

∗Corresponding author, Ph.D.
 E-mail: hosseini@iiees.ac.ir
[a]Ph.D. Student
 E-mail: Reza.Milanchian@gmail.com
[b]Ph.D.
 E-mail: nekooei@srbiau.ac.ir

of MR damper for seismic response mitigation of adjacent multistory buildings involving passive-off, passive-on and semi-active control strategies was examined by Bharti *et al.* (2010). Nigdeli and Bekdas (2014) studied using optimally Tuned Mass Dampers (TMD) to decrease the displacement vibrations of structures in adjacent structures and two different designs of TMD were investigated. For reducing the pounding hazard between two adjacent buildings a fuzzy logic controller was employed by Abdeddaim *et al.* (2016) to synchronize the response of structures coupled with MR dampers. Abdeddaim *et al.* (2016) showed that a coupling strategy can transform the vibrational mode of two separated structures into an individual system. Dumne *et al.* (2017) proposed two hybrid controls of coupled buildings connected with MR dampers in combination with Friction Pendulum System and Resilient Friction Base Isolator. They indicated that Hybrid controls are more effective in response reduction compared to Semi-active control.

A specific type of vertical isolation, called 'mass isolation' proposed by Ziyaeifar (2000) in which the isolation layer was applied in between of the mass and the lateral stiffness of the structure. The structural system was divided into two parts, one called the mass subsystem which contains the majority of the system's mass, and the other called the stiffness subsystem, which contains the majority of the system's stiffness. Nekooei and Ziyaeifar (2008) used 'mass seismic isolation' and also 'vertical mass isolation' for the formerly called 'mass isolation' idea. By those studies, the ability of mass isolation techniques in reducing earthquake effects on buildings with two parametric and numerical approaches was demonstrated. Nekooei and Ziyaeifar (2008) also studied the spectral response of the isolated structures and showed a significant decrease in earthquake input force in comparison to non-isolated structures. Ziyaeifar *et al.* (2012) introduced a two degrees of freedom model for mass isolation which was an extension of the Maxwell three-element type to improve the accuracy of structural mechanism that supports the reaction forces of large energy dissipating devices.

The main feature of the VSI in comparison to adjacent structures is that, response and characteristics of the vertically isolated structures (VIS) are evaluated relative to not only unconnected individual structures, but also to that of the original structure. This way of approaching the problem, makes VSI a feasible response reduction technique in design of structures. In the VSI, due to three-dimensionally behavior of the structure, the vertical isolation layers should be applied in a way to partition the structure into two inner and outer substructures. However, for investigating into fundamental features of our work, considering two-dimensional shear type structures is presumably adequate. It should be noted that in the present study, by partitioning an individual structure intentionally into two dynamically different substructures and linking them together by viscous or visco-elastic links, response reduction relative to the original structure was investigated. Numerous ratios were considered for mass and stiffness of either of the two substructures to the mass and stiffness of the original structure to find out which ratios or range of ratios result in maximum seismic response reduction.

Depending on these mass and stiffness ratios, three states of Mass Isolation, Interactional State, and Control Mass were differentiated in isolation behavior. Response history analyses were performed by Runge-Kutta numerical method. These analyses were carried out for several earthquakes. Color contour graphs were employed for presentation and investigation of large amounts of output results. Having results of both stiff and flexible isolated substructures in one individual graph provided considerably significant insight into the vertically isolated behavior. In these analyses, the relation between isolation ratios and link's damping and stiffness was also studied.

2. Analytical model of vertically isolated 1-story frame

In the VSI, a structure is partitioned into two interactional substructures in a vertical isolation layer by viscous or visco-elastic link dampers as shown in Fig. 1.

The Kelvin model is employed to represent the visco-elastic damper for which the stiffness and the damping coefficients are k_l and c_l respectively. Mass and stiffness of the original system are represented by m and k. Partitioning takes place in a way to have $m = m_1 + m_2$ and $k = k_1 + k_2$ in which subscripts 1 and 2 denote to be isolated structures. Inherent damping of the original system is considered as 2% of critical damping, so damping coefficient for the original model is $c = 0.04\, m\, \omega_n$. Also, as the damping ratio is preserved the same in each of individual substructures, we have $c_1 = 0.04\, m_1 \omega_1$ and $c_2 = 0.04\, m_2 \omega_2$, in which ω_1 and ω_1 are the natural frequencies of single substructures. The isolated one-story frame can be considered as two SDOF connected structures, and therefore, the governing equation of motion of the VIS subjected to earthquake horizontal excitations is as follows

$$
\begin{bmatrix} m_1 & 0 \\ 0 & m_2 \end{bmatrix} \begin{Bmatrix} \ddot{x}_1 \\ \ddot{x}_2 \end{Bmatrix} + \begin{bmatrix} c_1 + c_l & -c_l \\ -c_l & c_2 + c_l \end{bmatrix} \begin{Bmatrix} \dot{x}_1 \\ \dot{x}_2 \end{Bmatrix}
$$
$$
+ \begin{bmatrix} k_1 + k_l & -k_l \\ -k_l & k_2 + k_l \end{bmatrix} \begin{Bmatrix} x_1 \\ x_2 \end{Bmatrix} \qquad (1)
$$
$$
= - \begin{bmatrix} m_1 & 0 \\ 0 & m_2 \end{bmatrix} \begin{Bmatrix} 1 \\ 1 \end{Bmatrix} \ddot{x}_g
$$

in which x_1 and x_2 are relative displacements in isolated structures with respect to the ground and $\ddot{x}_g$ is the ground acceleration.
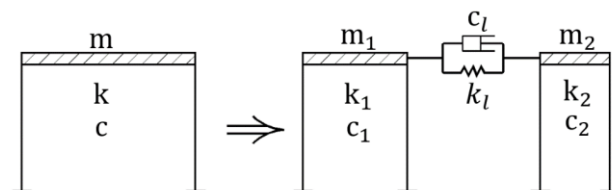

Fig. 1 The VSI concept in 1-story frame model partitioned into two substructures interconnected by a link

3. Dynamic characteristics of the VIS

In the VIS using visco-elastic dampers, system damping matrix will include the features of structural inherent damping as well as the added devices damping properties. Therefore, damping matrix of such a system would not be proportional damping. To decompose the set of differential equations of motion of the system, which is

$$M\ddot{x} + C\dot{x} + Kx = -M1\ddot{x}_g \qquad (2)$$

where M, K and C are mass, stiffness and non-classical damping matrices; 1 is a vector with each element equal to unity; x is the relative displacement vector with respect to the ground; assuming the dynamic response vector of the system as $x(t) = \Phi e^{\lambda t}$, results in

$$\lambda^2 M\phi + \lambda C\phi + K\phi = 0 \qquad (3)$$

where λ and ϕ are eigenvalue and eigenvector of the system. In the case of non-classical damping, one recognized approach for converting quadratic Eq. (3) to a linear one is using the augmented matrices as

$$\lambda \begin{bmatrix} 0 & M \\ M & C \end{bmatrix} \begin{Bmatrix} \lambda\phi \\ \phi \end{Bmatrix} + \begin{bmatrix} -M & 0 \\ 0 & K \end{bmatrix} \begin{Bmatrix} \lambda\phi \\ \phi \end{Bmatrix} = 0 \qquad (4)$$

The Eq. (4) can be rewritten in the familiar eigenvalue problem as

$$(-A^{-1}.B)\,\psi = \lambda\,\psi \qquad (5)$$

where $= \begin{bmatrix} 0 & M \\ M & C \end{bmatrix}$; $B = \begin{bmatrix} -M & 0 \\ 0 & K \end{bmatrix}$ and $\psi = \begin{Bmatrix} \lambda\phi \\ \phi \end{Bmatrix}$

There will be $2n$ eigenvalues for the n degrees of freedom system, corresponding to $2n$ eigenvectors. Eigenvalues will be in the form of complex-conjugate or real-valued pairs for underdamped or overdamped (mixed-damped) systems respectively, as discussed hereinafter.

3.1 Underdamped systems

In case of underdamped systems, all $2n$ eigenvalues and eigenvectors are complex-conjugate pairs with negative real parts, which can be written as (Zhang and Xu 1999)

$$\lambda_j = \bar{\lambda}_{j+n} \quad , \quad \phi_j = \bar{\phi}_{j+n} (j = 1,2, ..., n) \qquad (6)$$

$$\lambda_j = \bar{\lambda}_{j+n} = -\omega_j\xi_j + i\omega_{dj}(j = 1,2, ..., n) \qquad (7)$$

in which ω_j, ξ_j and ω_{dj} are natural frequency, damping ratio and damped frequency of jth mode and are calculated as

$$\omega_j = |\lambda_j|, \ \xi_j = -\frac{Rel(\lambda_j)}{|\lambda_j|} \ , \ \omega_{dj} = \omega_j\sqrt{1 - \xi_j{}^2} \qquad (8)$$

3.2 Mixed-damped systems

For the VIS, connected to each other by large damping dampers, solving characteristics equation may lead, in addition to the complex conjugate pairs, to some real-valued negative eigenvalues which each is associated with a real-valued eigenvector. In such cases, the system is called mixed-damped system, and its real-valued negative eigenvalues can be written as n pairs in the following form

$$\lambda_j = -\omega_j\xi_j + \omega_{dj}(j = 1,2, ..., n') \qquad (9)$$

$$\lambda_{j+n} = -\omega_j\xi_j - \omega_{dj}(j = 1,2, ..., n') \qquad (10)$$

in which $n' \leq n$ is the number of modes of the system with real eigenvalues and the values of ξ_j are all equal to or greater than one. From Eqs. (9)-(10) the real-valued undamped and damped pseudo-frequencies, as well as damping ratios are obtained as

$$\omega_j = \sqrt{\lambda_j\lambda_{j+n}}, \qquad \xi_j = -\frac{(\lambda_j + \lambda_{j+n})}{2\omega_j} \qquad (11a)$$

$$\omega_{dj} = \omega_j\sqrt{\xi_j{}^2 - 1} \qquad (11b)$$

4. Vertical isolation contour graph and performance states of the VSI

Since a significant number of different mass and stiffness ratios were considered in this study, an appropriate and comprehensive method for presentation and investigation of the output results was of great importance. In particular, these input and output data should include those related to both parts of the isolated structures. One of the common methods to show this kind of combined input and output data in which the output is a function of two variables is using curved surface in a three-dimensional Cartesian coordinate system. Mass and stiffness ratios should be taken into account simultaneously for better understanding of isolation effects, therefore; three-dimensional Cartesian coordinate system was utilized in which horizontal coordinates axes were set as the stiffness and mass ratios and the vertical axis was considered for representing the seismic response or any other desired output such as damping ratio. Although the three-dimensional representation of the curved surface is useful, a full understanding of minimal and maximal values is not convenient. Consequently, it was preferred to present the results as a color contour graph which is a different demonstration of the three-dimensional curved surface. The more important advantage of this representation is creating the possibility to observe the results of both stiff and flexible isolated structures in one individual graph. This provides more appropriate insight into the behavior of the VIS. Mass and stiffness ratios for flexible substructure were defined as $\alpha_{m1} = m_1/m$ and $\alpha_{s1} = k_1/k$, and those of stiff substructure as $\alpha_{m2} = 1 - \alpha_{m1}$ and $\alpha_{s2} = 1 - \alpha_{s1}$, so that their summation is always equal to unity. On this basis, if values of α_{s1} and α_{m1} are shown respectively on horizontal and vertical axes, the results corresponding to the stiff substructure are in central symmetry relative to those of flexible substructure, as the center point of the graph

corresponds to $\alpha_m = 0.5$ and $\alpha_s = 0.5$.

From now on, this graphical representation is called vertical isolation contour graph (VICG). The area at the left and above of the main diagonal of the graph rectangle (the upper triangle - referred to as TUT from now on) corresponds to flexible substructures while the area at the right and below that main diagonal (the lower triangle - referred to as TLT from now on) corresponds to stiff substructures. In either side of the diagonal of the graph and parallel to it, middle areas between the diagonal and upper left and lower right corners are related to an interactional state of the VSI, while areas close to those two corners are related to mass isolation state. Furthermore, there is a small area of interactional states area at the left lower corner of TUT, which could be interpreted as control mass state.

5. Effects of link parameters on modal characteristics of the VIS

To have a better understanding of the VSI features, initially, a numerical study of a sample 1-story single frame is considered to be helpful. In this basic sample, the story mass was assumed as 100 ton and the lateral stiffness as 10,000 kN/m. This stiffness value was assigned such that the maximum drift, determined by static equivalent lateral force procedure in the high seismic zone, was limited to the seismic design code specified value.

In the VIS by using viscous or visco-elastic dampers, the influence of system dynamic characteristics, including natural frequencies and modal damping ratios in response reduction are of interest. In a comprehensive study, for different mass and stiffness ratios that could be assigned to either part of the isolated structure, eigenvalue analyses of the non-classically damped system were performed. These analyses also have been carried out for different parameters of the connecting link. Evidently, investigation on the link parameters, including damping and stiffness, should be done in a reasonable range. A value of 30% of the critical damping is a practical upper limit for combined viscous and structural damping. Out of this 30% damping at most 25% is viscous damping and the remaining 5% is structural damping (Lee and Taylor 2001). Hence, an estimate of the maximum amount of added link damping to reach the maximum reasonable practical damping ratio of about 20% of the original structure is calculated as $c_{max} = 2 \times 100 \times$

$10 \times 0.2 = 400\ \mathrm{kN\ s/m}$. The lower amount of added link damping was considered as $c_{min} = 100\ \mathrm{kN\ s/m}$ that corresponds to the damping ratio of 5% in the original structure. The link parameters can be expressed in a more appropriate manner with respect to the original structure features as

$$\xi_l = \frac{c_l}{2m\omega_n}\ ,\qquad \beta_l = \frac{k_l}{k} \tag{12}$$

Based on the numerical conducted analyses, results of modal damping ratios of various states of the VIS are shown in following figures in the VICG. To have a proper intuition of the dynamic characteristics of the VIS, in addition to practical values of stiffness and damping, results corresponding to very large and excessive stiffness and damping values were also considered and investigated.

In Fig. 2 modal damping ratios of the first and second modes of single-story VIS with a viscous link, for different stiffness and mass ratios of flexible substructure, (α_{s1} and α_{m1}) are shown for three different values of the link parameter. In these VICG presentations, the main diagonal has been considered as the border between results corresponding to the first and the second mode respectively. For a given pair of α_{s1} and α_{m1} values, modal damping ratio of the first mode is indicated by a point above the main diagonal whose centrally symmetric point corresponds to the modal damping ratio of the second mode.

An interesting finding of the VICGs presented in Fig. 2, is their symmetry with respect to the main diagonal. The reason of this symmetry is that for any two reciprocal pairs of α_{s1} and α_{m1} the modal damping values are also reciprocally the same, although the frequency values may not be reciprocally the same. This point can be better understood by looking at the damping values shown in Table 1.

According to Figs. 2(a)-(c) it is clear that an increase in the link damping ratio leads to an increase in modal damping ratios of both modes of the VIS, however, the increase levels are not the same for different stiffness and mass ratios and one of the damping ratios is always greater than the other. Greater modal damping ratio could occur in either first or second mode. The greater modal damping ratio grows too fast and is prone to critical and over-critical damping values, while the other modal damping ratio grows slowly and never tends to reach critical damping, and it


(a) $\xi_l = 5\%$　　　　　(b) $\xi_l = 10\%$　　　　　(c) $\xi_l = 20\%$
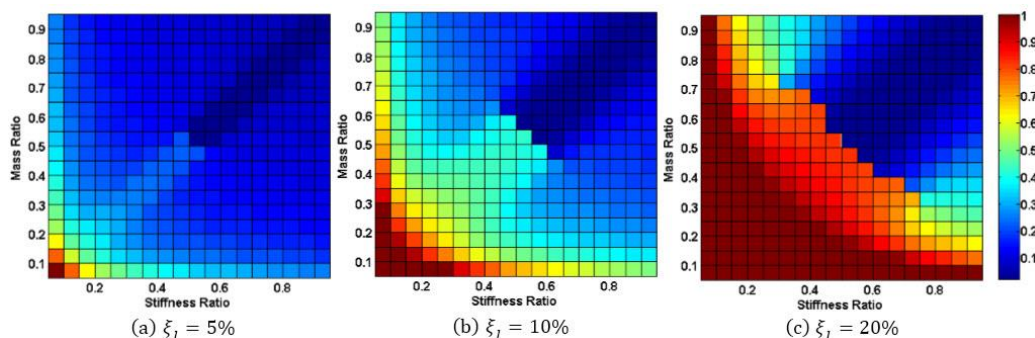
Fig. 2 Modal damping ratios in the VIS interconnected by a viscous link

(a) $\xi_l = 20\%, \beta_l = 0.05$ (b) $\xi_l = 20\%, \beta_l = 0.2$ (c) $\xi_l = 20\%, \beta_l = 0.5$
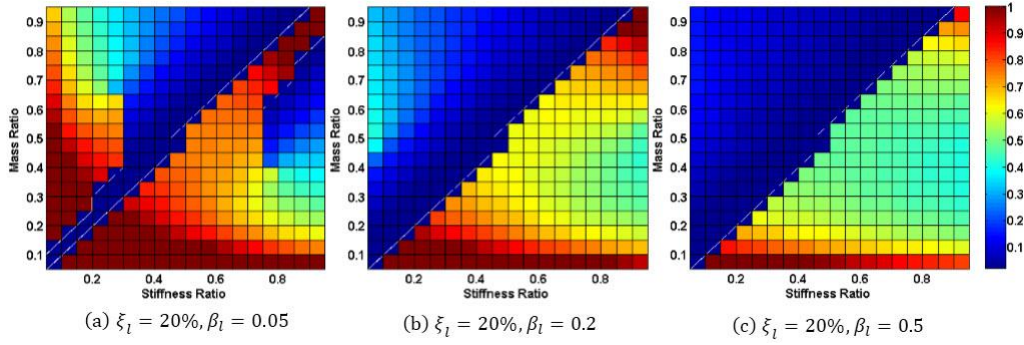
Fig. 3 Modal damping ratios in the VIS interconnected by a visco-elastic link with a constant damping value

(a) $\xi_l = 5\%, \beta_l = 0.1$ (b) $\xi_l = 10\%, \beta_l = 0.1$ (c) $\xi_l = 20\%, \beta_l = 0.1$
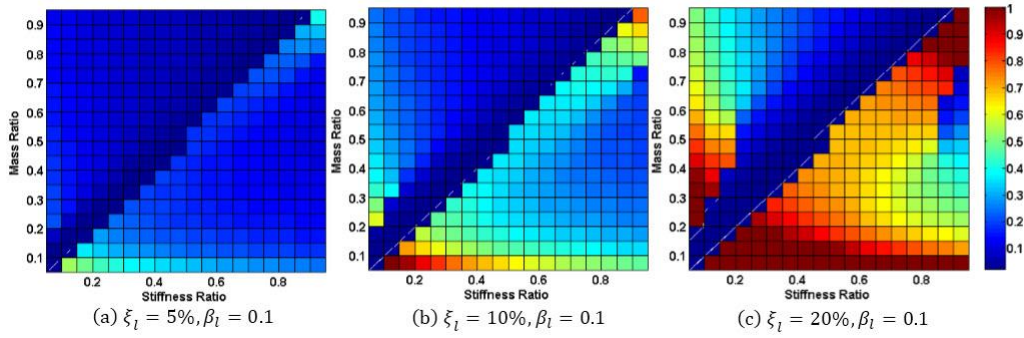
Fig. 4 Modal damping ratios in the VIS interconnected by a visco-elastic link with a constant stiffness value

(a) $\xi_d = 10\%, \beta_d = 0$ (b) $\xi_d = 40\%, \beta_d = 0$ (c) $\xi_d = 10\%, \beta_d = 0.5$
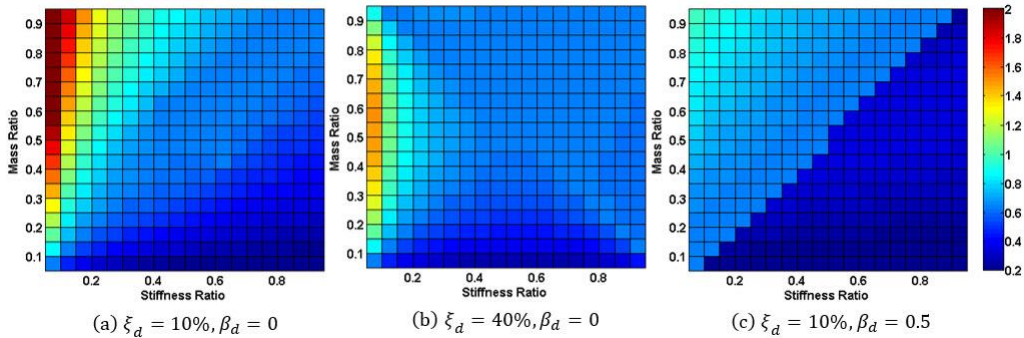
Fig. 5 Natural modal period values in the VIS by viscous and visco-elastic link

Table 1 Samples of numerical results of modal damping ratios in the VIS by viscous link parameter of $\xi_l = 20\%$

		α_{s1}								
		0.1	**0.2**	**0.3**	**0.4**	**0.5**	**0.6**	**0.7**	**0.8**	**0.9**
	0.1	2.242	1.675	1.425	1.266	1.140	1.027	0.923	0.836	0.769
	0.2	1.675	1.270	1.099	0.991	0.901	0.805	0.678	0.583	0.531
	0.3	1.425	1.099	0.972	0.899	0.841	0.784	0.299	0.418	0.401
	0.4	1.266	0.991	0.899	0.853	0.824	0.073	0.149	0.247	0.292
α_{m1}	**0.5**	1.140	0.901	0.841	0.824	0.020	0.033	0.072	0.136	0.197
	0.6	1.027	0.805	0.784	0.801	0.033	0.020	0.032	0.070	0.121
	0.7	0.923	0.678	0.697	0.149	0.072	0.032	0.020	0.032	0.066
	0.8	0.836	0.583	0.418	0.247	0.136	0.070	0.032	0.020	0.032
	0.9	0.769	0.531	0.401	0.292	0.197	0.121	0.066	0.032	0.020

even decreases to the inherent damping when link damping ratio becomes very large. This is the state in which the two substructures are actually locked together and is referred to locked mode (Ziyaeifar *et al.* 2012). In the practical range

of link damping, if $\alpha_{s1} + \alpha_{m1} = 1$, the modal damping ratios for both modes will be the same. With an increase of the link damping, overdamped area tends to extend to all range of mass and stiffness ratios whose summation is less than unity (area below the minor diagonal of the VICG). This tendency can be seen in Fig. 2(c).

In the next stage, the modal damping in a single story VIS which is interconnected by visco-elastic link was investigated comprehensively by variation of both link damping and link stiffness. In a set of analyses for a certain link damping, link stiffness was considered to vary from practical to very large values, and dynamic characteristics were calculated for different mass and stiffness ratios. Fig. 3 shows the resulting modal damping ratios. As it is observed in Fig. 3, with an increase of the link stiffness ratio a shift of the greater modal damping ratio toward the second mode occurs, and simultaneously both modal damping ratios decrease (Figs. 3(a)-(b)). In the case of excessive values of link stiffness, link damping effects are reduced considerably, and damping ratio of the first mode reduces to the inherent damping (Fig. 3 (c)).

To study the effects of damping value of visco-elastic link on modal characteristics of the VIS for a certain value of link stiffness link damping was considered as a variable. The resulting modal damping ratios are shown in Fig. 4.

Comparing Fig. 2 and Fig. 4 it can be seen that, the existence of the link stiffness causes alteration of the modal damping ratios and also causes the greater modal damping to correspond to the second mode of the system. Looking at Fig. 4(c) one can realize that by an increase in the link damping value, both modal damping ratios increase; it is always possible to find mass and stiffness ratios by which the greater modal damping belongs to the first mode of the VIS, provided that the link stiffness value is small enough.

As shown in Fig. 5, representing natural periods in different mass and stiffness ratios in the VICG presentation can be beneficial for better understanding of the effects of link parameters on the dynamic behavior of the VIS.

In Fig. 5(a), for a moderate link damping value, a wide range of system natural periods are observed in the first and second mode of the VIS. Natural periods of the VIS for excessive link damping value is shown in Fig. 5(b). By increasing link damping value, first and second modal periods of the VIS approach the original structure's natural period, which is a state of system locked mode. In Fig. 5(c) natural periods of the VIS are presented in the case of link large stiffness value. As it is clear in this case, the first natural period of the system approaches the original structure's natural period, while the second natural period tends to stay in low period range, which is another state of system locked mode.

6. Seismic response of the VIS

To study the seismic performance of the 1-story VIS, it was subjected to different earthquake excitations and its response histories were obtained by a series of time history analysis (THA) cases. In these analyses, the aim was examining the effects of different parameters on the

efficiency of the VSI. In the VSI study, one of the main goals is to determine an appropriate range of mass and stiffness ratios and the associated interconnecting link parameters to achieve the maximum possible seismic response reduction. For this purpose, numerous analyses were carried out in this study on 1-story VIS of different mass and stiffness ratios.

In the VIS by viscous or visco-elastic links, the damping matrix is of non-classically damped type and assumption of Rayleigh damping is no longer valid, therefore. The damping matrix should be determined based on the considered interconnecting link characteristics. In this study, the State Space Vector technique was used to reduce differential equations order for the required solution. To solve numerically the governing differential equations of motion, a program was developed in MATLAB environment based on Runge-Kutta method by the authors.

The maximum displacement in response history of each isolated structures which is the most important seismic response parameter was selected as a criteria for seismic performance evaluation. Comparisons of maximum displacements of each substructure of the isolated structure with that of the original structure were taken into account as the VSI performance assessment. Response ratios for both flexible and stiff substructure were defined as

$$R_{\text{Flexible}} = \frac{\langle X_{\max}\rangle_{\text{Flexible}}}{\langle X_{\max}\rangle_{\text{Original}}}, \; R_{\text{Stiff}} = \frac{\langle X_{\max}\rangle_{\text{Stiff}}}{\langle X_{\max}\rangle_{\text{Original}}} \quad (13)$$

6.1 Ground motion selection

Regarding that the input earthquakes characteristics are influential in the results of any response history analysis, it has been attempted to select a wide range of earthquakes. As shown in Fig. 5 the natural periods of the 1-story VIS for different mass and stiffness ratios are scattered in a wide range. Moreover, dominant periods of earthquake records fall in different ranges of structural periods. As a result, it is likely that in mass and stiffness ratios, the VIS frequencies get the values close to the dominant frequency of an earthquake which leads to a resonance case. Hence, time history analyses results can be sensitive to the input earthquake excitation.

Herein, it was intended to select earthquakes in such a
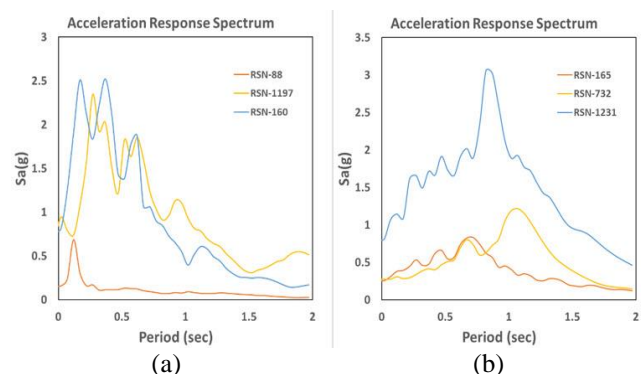
Fig. 6 Selected accelerations response spectra: (a) Group-1, (b) Group-2

(a) $\xi_l = 5\%$ (b) $\xi_l = 10\%$ (c) $\xi_l = 20\%$
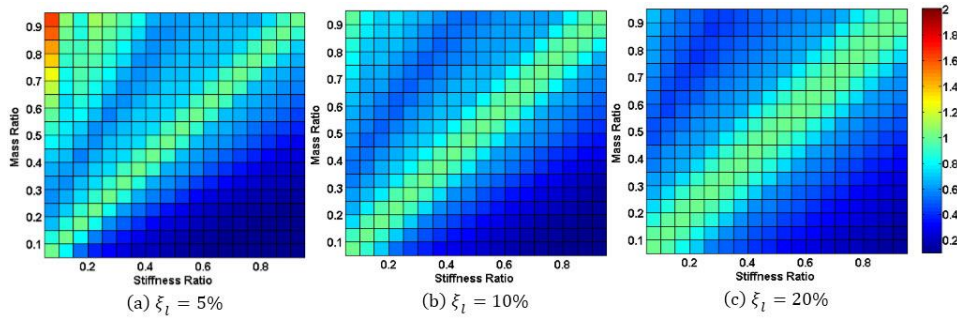
Fig. 7 Response ratios of the VIS for different viscous link parameters in RSN88_SFERN earthquake

(a) $\xi_l = 5\%$ (b) $\xi_l = 10\%$ (c) $\xi_l = 20\%$
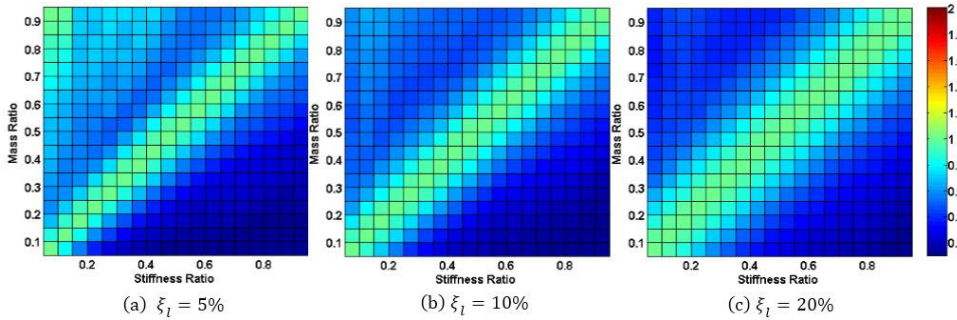
Fig. 8 Response ratios of the VIS for different viscous link parameters in RSN1197_CHICHI earthquake

(a) $\xi_l = 5\%$ (b) $\xi_l = 10\%$ (c) $\xi_l = 20\%$
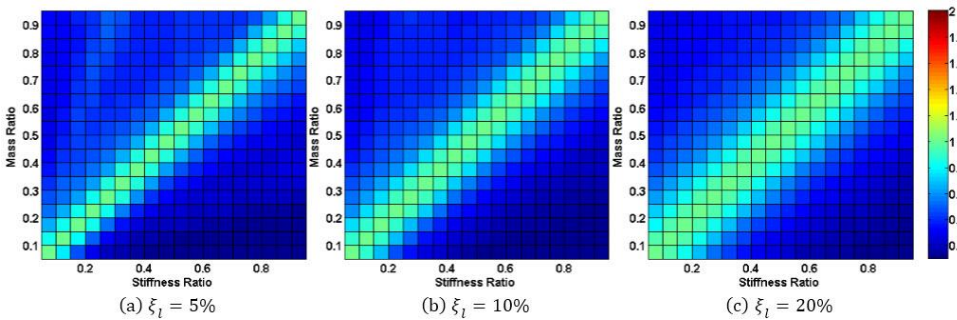
Fig. 9 Response ratios of the VIS for different viscous link parameters in RSN160_IMPVALL earthquake

way that their peak spectral acceleration falls in different time periods. In this study, since the assessment of the VSI efficiency was carried out by comparing responses of the isolated and the original structure independently for each earthquake, there was no need to scale the records. As shown in Fig. 6, these records have been classified into two different groups. The ones whose peak spectral accelerations lay in the period range of less than 0.5 seconds, considered as the earthquake events in the stiff site conditions (Group-1); and those ones whose peak spectral accelerations lay in the period range of greater than 0.5 seconds, usually represent the earthquake events occurring in soft soil conditions (Group-2).

6.2 Numerical results of the VIS seismic responses

As mentioned before, the VICG was used for presentation and investigation of large amounts of output results of this study. In this section, two cases of the viscous and visco-elastic link in the VIS were investigated. The output results presented by the VICG were response ratios of the two substructures of the VIS to that of the original structure. Regions in the plot area in which response ratio is less than unity represent the mass and stiffness ratios by which response reduction is achieved.

In Figs. 7-9, results of response calculations of the VIS interconnected by viscous links for selected earthquakes of Group-1 (short-period earthquakes) are demonstrated. For convenience, in the case of each earthquake, the results are presented for low, moderate and upper practical damping values of ξ_l (Eq. (12)). By investigating the VICGs, worthwhile insight into the VSI is created. In all of the presented graphs the main diagonal that separates the results of flexible and stiff substructures from each other is independent of interconnecting link parameters and it is also distinguished by response ratio of unity. In TLT area of the graph that is related to stiff substructure results, response ratios are considerably less than unity almost in all earthquakes and majority of mass and stiffness ratios. So, it is certain that the VSI is effective in stiff substructure and response ratio for this substructure is less dependent on link damping parameters. In TUT area of the graph which is

(a) $\xi_l = 5\%, \beta_l = 0.05$ (b) $\xi_l = 5\%, \beta_l = 0.1$ (c) $\xi_l = 5\%, \beta_l = 0.5$
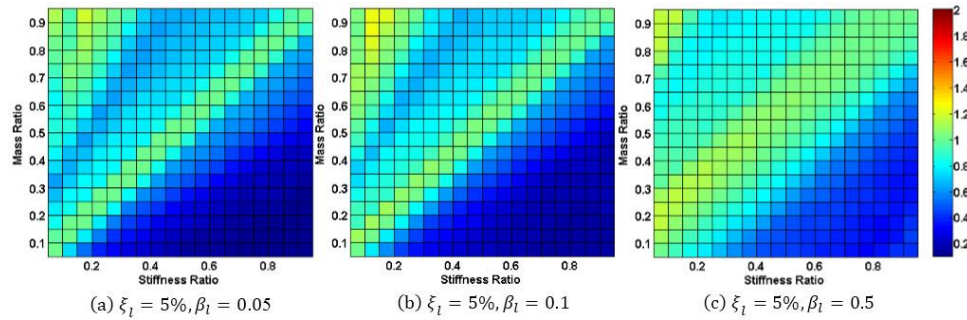
Fig. 10 Response ratios of the VIS for different visco-elastic link parameters in RSN88_SFERN earthquake

(a) $\xi_l = 5\%, \beta_l = 0.05$ (b) $\xi_l = 5\%, \beta_l = 0.1$ (c) $\xi_l = 5\%, \beta_l = 0.5$
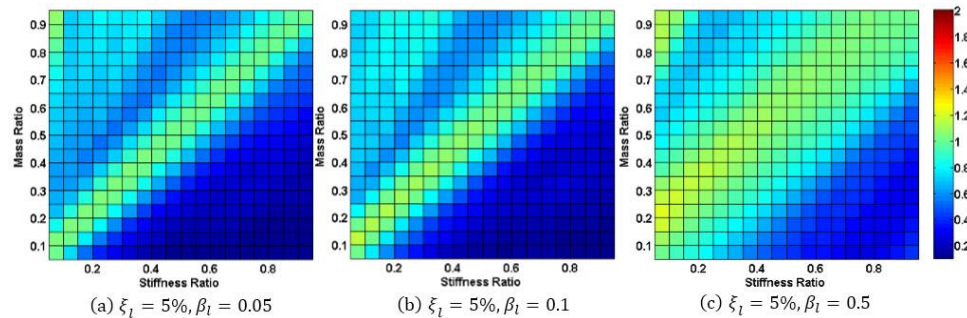
Fig. 11 Response ratios of the VIS for different visco-elastic link parameters in RSN1197_CHICHI earthquake

(a) $\xi_l = 5\%, \beta_l = 0.05$ (b) $\xi_l = 5\%, \beta_l = 0.1$ (c) $\xi_l = 5\%, \beta_l = 0.5$
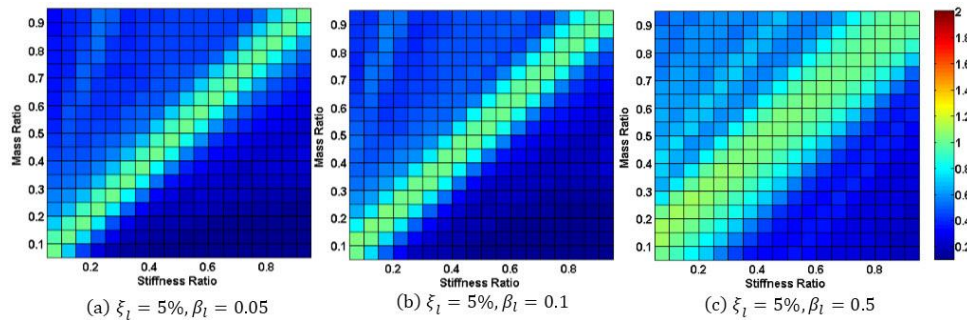
Fig. 12 Response ratios of the VIS for different visco-elastic link parameters in RSN160_IMPVALL earthquake

related to flexible substructure results, response ratios are more dependent on mass and stiffness ratios and the interconnecting link parameters. On this basis, the majority of discussion on the VIS is focused on flexible substructure from now on.

According to Figs. 7(a)-8(a) for the small link damping value ($\xi_l = 5\%$), area range of response ratios less than unity is first formed in the middle band of TUT parallel to the main diagonal. The trend of formation of the middle band with minimum response ratios indicates the appropriate structural interaction state in response reduction using small damping. By increasing interconnecting link damping, area range with response ratios less than unity spreads toward the vertical and horizontal edges of TUT and TLT. As the area corresponding to the minimum response ratios approaches the mentioned edges, mass isolation state is revealed (Figs. 7(b)-8(b)).

In Figs. 7(c)-8(c) results of response ratios related to upper practical values $\xi_l = 20\%$ are shown. In these figures, in both substructures, response reduction in the majority of mass and stiffness ratios are satisfactory, however; these response ratios vary with the values of

α_{s1} and α_{m1}. Also, for large values of ξ_l the sensitivity of response to α_{s1} and α_{m1} decreases. In addition to α_{s1} and α_{m1}, response ratios of the VIS are also influenced significantly by earthquake characteristics. In the case of RSN160_IMPVALL earthquake, response reduction for all α_{s1} and α_{m1} values, regardless of link damping value, is really stunning as shown in Fig. 9.

The question may be aroused if there is any relation between the modal damping ratios of the VIS (Fig. 2) and the corresponding response reduction amounts, shown in Figs. 7-9. In fact, by investigating these figures, one cannot gain any explicit insight into their relation. Based on the response reduction results, greater modal damping for a set of α_{s1} and α_{m1} does not lead necessarily to more response reduction in the VIS. However, it is clear that the link damping value does have direct effects on seismic response reduction of the VIS, especially in flexible substructure.

Figs. 10-12 show the response ratios of the VIS interconnected by a visco-elastic link subjected to selected earthquakes of group-1 for various values of link stiffness,

(a) $\xi_l = 5\%$ (b) $\xi_l = 10\%$ (c) $\xi_l = 20\%$
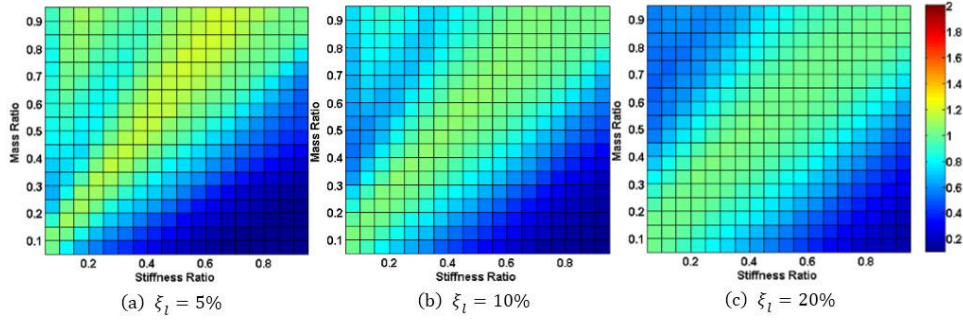
Fig. 13 Response ratios of the VIS for different viscous link parameters in RSN165_IMPVALL earthquake

(a) $\xi_l = 5\%$ (b) $\xi_l = 10\%$ (c) $\xi_l = 20\%$
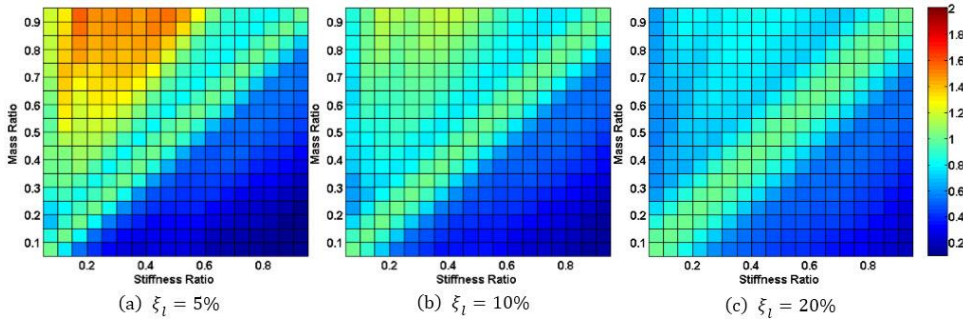
Fig. 14 Response ratios of the VIS for different viscous link parameters in RSN1231_CHICHI earthquake

(a) $\xi_l = 5\%$ (b) $\xi_l = 10\%$ (c) $\xi_l = 20\%$
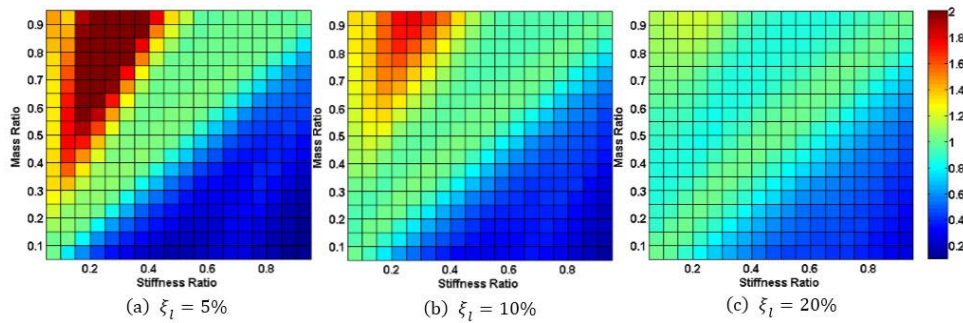
Fig. 15 Response ratios of the VIS for different viscous link parameters in RSN732_LOMAP earthquake

β_l. As shown in Figs. 10(a), 10(b)-12(a), 12(b), the stiffness of link has different influences on responses of the two substructures. Response reduction in stiff substructure is not changed considerably due to the link stiffness in practical range, even it can be observed that for values of link stiffness $\beta_l = 0.05$ and $\beta_l = 0.1$ more response reduction is achieved. By increasing the link stiffness to high ranges, the efficiency of the visco-elastic link on response reduction is decayed gradually (Figs. 10(c)-12(c)).

In flexible substructure, link stiffness distinctly alter the response with different α_{s1} and α_{m1} values. In the middle band area of TUT which corresponds to interactional state, stiffness of link somehow leads to less response reduction in comparison to viscous link for the practical values of stiffness (Figs. 10(a), 10(b)-12(a), 12(b)). However, in the mass isolation state, seismic response of flexible substructure could be improved by employing visco-elastic link.

As a matter of fact, link stiffness reduces damping effect of the link and consequently, affects response ratio of flexible substructure, especially in the interactional state.

Yet, in small and practical values of link stiffness ($\beta_l < 0.1$), its influence is not much remarkable. Link stiffness reduces significantly the link damping efficiency in both substructures for large values (Figs. 10(c)-12(c)).

Response ratios for selected earthquakes of Group-2 (long-period earthquakes) are presented in Figs. 13-15 in the VICG format. They show that the response of stiff substructure in the VSI is not much dependent on α_{s1} and α_{m1} values as well as link parameters and earthquake excitation characteristics which is similar to earthquakes of Group-1. According to the resulting VICGs, response ratios of flexible substructure are more dependent on input earthquakes characteristics and their performance is not generally as satisfactory as their performance subjected to earthquakes of Group-1. This can be justified by paying attention to acceleration response spectrum of selected earthquakes of Group-2 in Fig. 6 and their more accordance with the period of the first mode of the VIS, shown in Fig. 5.

According to Figs. 13-14 for having acceptable response ratios in the VIS for a wide range of isolation ratios, it is
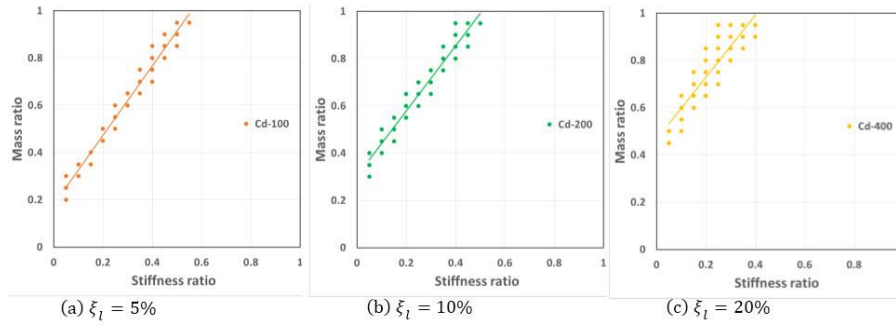
Fig. 16 Optimal isolation ratios and their corresponding trend lines for the VIS with viscous link in the case of RSN88_SFERN earthquake
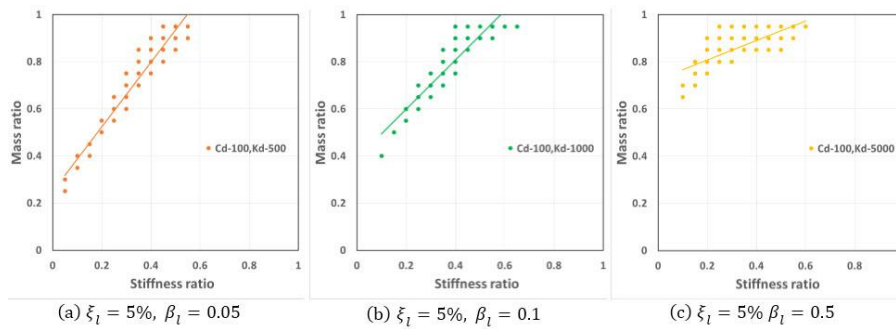
Fig. 17 Optimal isolation ratios and their corresponding trend lines for the VIS with visco-elastic link in the case of RSN88_SFERN earthquake
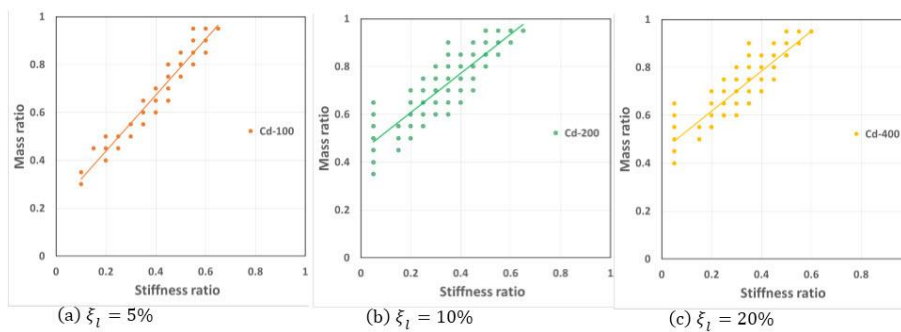
Fig. 18 Optimal isolation ratios and their corresponding trend lines for the VIS with viscous link in the case of RSN1231_CHICHI earthquake
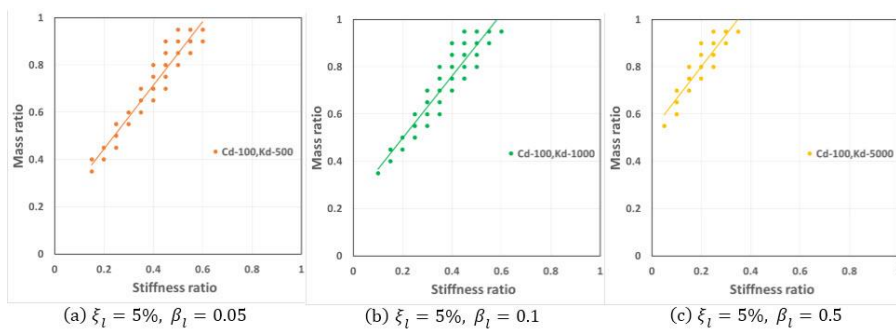
Fig. 19 Optimal isolation ratios and their corresponding trend lines for the VIS with visco-elastic link in the case of RSN1231_CHICHI earthquake

inevitable to use moderate practical values or larger of link damping. However, like any vibrational system subjected to an arbitrary excitation, it is probable not to meet the desired response ratios in the VIS, unless the larger practical values

of link damping is used, as shown in Fig. 15. Results of the case with a visco-elastic link, presented in the main report of the study (Milanchian 2017), are similar to those of the case with a viscous link and are not presented here for

Table 2 Mean and Standard Deviation values of the desired selected response ratios in the case of RSN88_SFERN earthquake

		Viscous Damper						Visco-Elastic Damper				
$\xi_l(\%)$	QTY	α_{s1}	α_{m1}	$R_{Flexible}$	R_{Stiff}	$\xi_l(\%)$	β_l	QTY	α_{s1}	α_{m1}	$R_{Flexible}$	R_{Stiff}
5	Value	0.30	0.62	0.6	0.38	5	0.05	Value	0.32	0.69	0.65	0.28
	SD	0.15	0.23	0.02	0.17			SD	0.14	0.20	0.02	0.13
10	Value	0.26	0.67	0.53	0.35	5	0.10	Value	0.37	0.78	0.68	0.22
	SD	0.14	0.19	0.02	0.11			SD	0.13	0.15	0.02	0.06
20	Value	0.22	0.76	0.46	0.31	5	0.5	Value	0.33	0.86	0.79	0.39
	SD	0.10	0.15	0.02	0.07			SD	0.14	0.08	0.02	0.04

Table 3 Mean and Standard Deviation values of the desired selected response ratios in the case of RSN1231_CHICHI earthquake

		Viscous Damper						Visco-Elastic Damper				
$\xi_l(\%)$	QTY	α_{s1}	α_{m1}	$R_{Flexible}$	R_{Stiff}	$\xi_l(\%)$	β_l	QTY	α_{s1}	α_{m1}	$R_{Flexible}$	R_{Stiff}
5	Value	0.40	0.67	0.53	0.35	5	0.05	Value	0.39	0.71	0.57	0.26
	SD	0.16	0.19	0.02	0.13			SD	0.13	0.18	0.02	0.11
10	Value	0.32	0.71	0.48	0.29	5	0.10	Value	0.37	0.72	0.60	0.23
	SD	0.16	0.15	0.02	0.09			SD	0.12	0.17	0.02	0.06
20	Value	0.32	0.71	0.48	0.29	5	0.5	Value	0.20	0.80	0.69	0.30
	SD	0.16	0.15	0.02	0.09			SD	0.08	0.12	0.023	0.02

brevity. Generally speaking, in the VSI, selection of wider range of α_{s1} and α_{m1} will be possible, if larger values of damping are used in both viscous and visco-elastic links.

7. Optimal ranges of stiffness and mass ratios in the VIS

Although the VICGs provide information and good understanding about behavior and response control of the VIS qualitatively, quantitative and numerical analysis of isolation behavior is of a great importance, particularly, for suggesting more appropriate α_{s1} and α_{m1} values for various link parameters considering the objective of the VSI. For every presented VICG, since response ratios in VICGs are scattered in ranges larger and less than unity, values of α_{s1} and α_{m1} were considered, for which response ratios in both substructures are less than unity. Paying attention to the dispersion of eligible response ratios, a series of desired of α_{s1} and α_{m1} pairs with minimal response ratios were selected. Distribution of selected of α_{s1} and α_{m1} values is depicted in an Isolation Ratios Coordinate System (IRCS) to make it possible to find the trend of corresponding curves of optimal ratios. In Figs. 16-19 the desired outcomes of conducted analyses for different parameters of viscous and visco-elastic links for two of selected earthquakes of Group-1 (short-period earthquakes) are demonstrated in the IRCS.

Summary of the results obtained from Figs. 16-17, including the average values of isolation ratios as well as the mean and Standard Deviation values of the response ratios in both stiff and flexible substructures for different link parameters are presented in Table 2.

Similar results of optimal values of the isolation ratios for other earthquake of Group-1 (short-period earthquakes) are shown in Figs. 18-19 and the corresponding statistical values are given in Table 3.

As it is observed in Figs. 16-19 and Tables 2-3, investigating the VSI behavior in multiple earthquakes yields to some distinct performances which aid the selection of practical isolation ratios as well as appropriate link type and its optimal parameters. As shown in Figs. 16-19 the trend lines of optimal isolation ratios are mostly the lines with slopes of near unity in the IRCS for most of the employed earthquakes. This feature provides numerous selections of mass and stiffness ratios especially with small or moderate link damping values in the interactional state.

According to the results presented in Tables 2-3, the average value of the response reduction factors in the case of short-period earthquakes is quite remarkable, particularly for the VIS with a viscous link. With gradual increase of link damping value, the points corresponding to the optimal values of isolation ratios shift toward the upper left corner of the IRCS graph area, where 'mass isolation state' could be revealed, although the interactional state is still sustained (Fig. 16 (c) and Fig. 18(c)).

From Fig. 17 and Fig. 19 it can be observed that, in the VIS, interconnected by visco-elastic links, optimal coordinates of isolation ratios shift toward the upper left corner of the IRCS graph area by an increase in the link stiffness. This shifting denotes the mass isolation state approach and accordingly, the response ratios of both flexible and stiff substructures change. According to Tables 2-3, the changes in response ratios are as follow. In practical range of the link stiffness $\beta_l < 0.1$, increasing the link stiffness causes a decrease in the response ratio of stiff

(a) $\xi_l = 5\%$ (b) $\xi_l = 10\%$ (c) $\xi_l = 20\%$
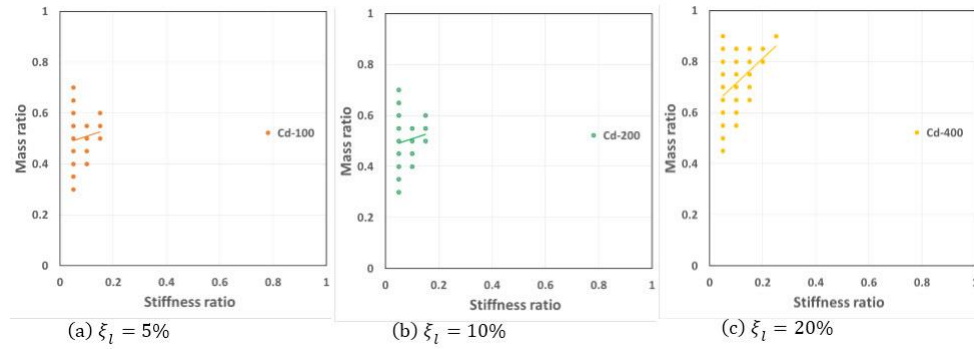
Fig. 20 Optimal isolation ratios and their corresponding trend lines for the VIS with viscous link in the case of RSN165_IMPVALL earthquake


(a) $\xi_l = 5\%$, $\beta_l = 0.05$ (b) $\xi_l = 5\%$, $\beta_l = 0.1$ (c) $\xi_l = 5\%$, $\beta_l = 0.5$
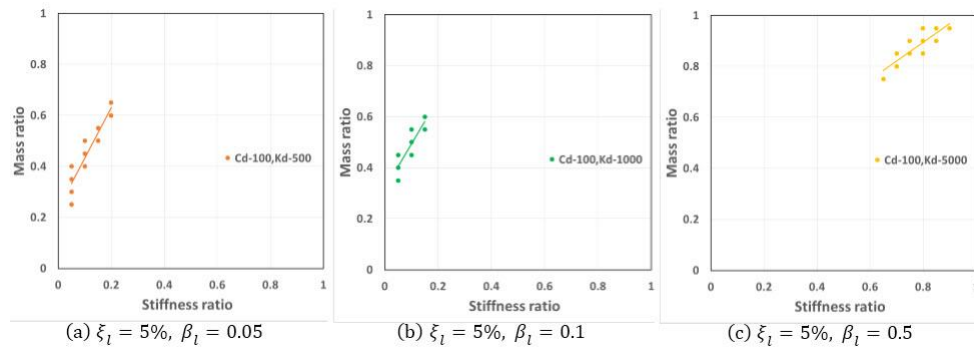
Fig. 21 Optimal isolation ratios and their corresponding trend lines for the VIS with visco-elastic link in the case of RSN165_IMPVALLearthquake

Table 4 Mean and Standard Deviation values of the desired selected response ratios in the case of RSN165_IMPVALL earthquake

		Viscous Damper						Visco-Elastic Damper				
$\xi_l(\%)$	QTY	α_{s1}	α_{m1}	$R_{Flexible}$	R_{Stiff}	$\xi_l(\%)$	β_l	QTY	α_{s1}	α_{m1}	$R_{Flexible}$	R_{Stiff}
5	Value	0.11	0.38	0.74	0.55	5	0.05	Value	0.11	0.45	0.88	0.43
	SD	0.055	0.099	0.045	0.077			SD	0.06	0.12	0.03	0.09
10	Value	0.08	0.50	0.61	0.44	5	0.10	Value	0.09	0.48	0.97	0.34
	SD	0.04	0.11	0.04	0.12			SD	0.04	0.08	0.01	0.06
20	Value	0.10	0.72	0.55	0.33	5	0.5	Value	0.78	0.88	0.98	0.83
	SD	0.056	0.124	0.025	0.104			SD	0.07	0.06	0.01	0.06

Table 5 Dynamic characteristics of the original 5-story building model

Mode/Story No.	**m** (ton)	**k** (kN/m)	**ω** (rad/sec)	**T** (sec)	**M*** (kg)
1	100	45000	5.53	1.136	417.74
2	100	40000	14.48	0.434	52.25
3	100	35000	22.52	0.279	18.34
4	100	30000	29.92	0.210	7.73
5	100	20000	36.31	0.173	3.91

substructure and also causes an increase in the response ratio of flexible substructure, although this ratio still remains in the satisfactory range.

The trend lines shown in Figs. 16-19 can be used as a preliminary design tool for new buildings to benefit from the interactional state of the VSI. In general, these trend lines have the following equation

$$\alpha_{m1} = m'.\alpha_{s1} + b \quad (14)$$

in which m' is the slope and b is the latitude of the line. For the link parameters of practical range, namely $0.05 < \xi_l < 0.2$ and $\beta_l < 0.1$, the appropriate initial design values for m' and b are suggested as

(a) $RSN88\_SFERN$

(b) $RSN160\_IMPVALL$

(c) $RSN1197\_CHICHI$

(d) $RSN165\_IMPVALL$

(e) $RSN732\_LOMAP$

(f) $RSN1231\_CHICHI$
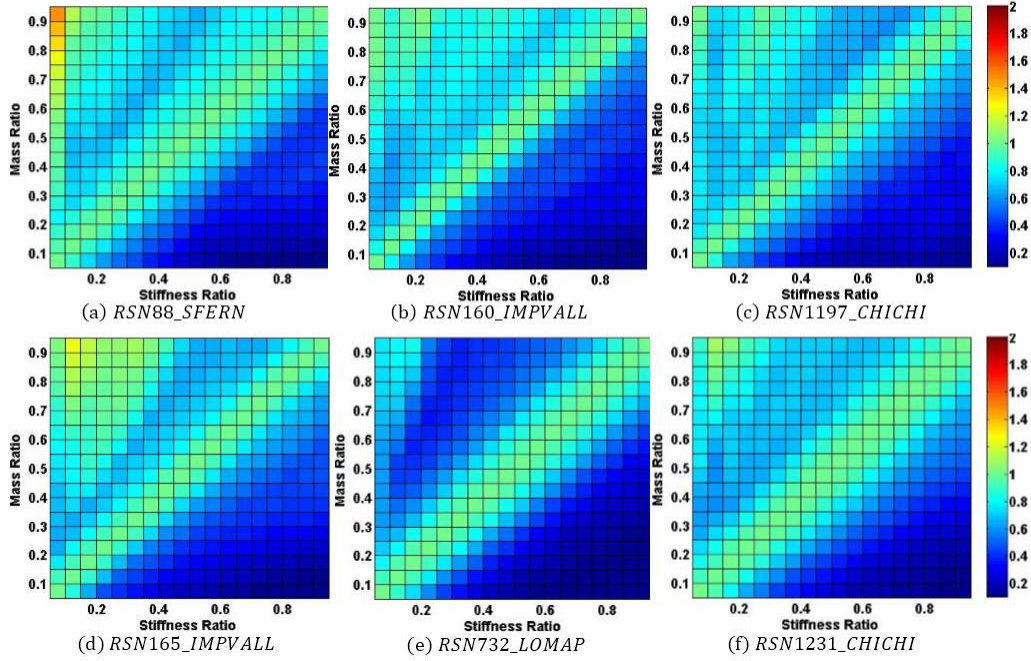
Fig. 22 Response ratios of the 5-story VIS interconnected by viscous links with $\xi_l = 10\%$ for selected earthquakes

Table 6 Numerical results of the 5-story building with different isolation ratios subjected to selected earthquakes of Group-1

	α_{s1}	α_{m1}	β_l	$\xi_l(\%)$	RSN88_SFERN		RSN160_IMPVALL		RSN1197_CHICHI	
					$R_{Flexible}$	R_{Stiff}	$R_{Flexible}$	R_{Stiff}	$R_{Flexible}$	R_{Stiff}
Interactional State	0.25	0.5	0	5	0.75	0.50	0.90	0.49	1.02	0.67
				10	0.66	0.57	0.73	0.44	0.82	0.60
				20	0.70	0.66	0.63	0.47	0.65	0.65
			0.1	10	0.81	0.52	0.77	0.44	0.86	0.53
	0.4	0.6	0	5	0.86	0.57	0.82	0.46	0.89	0.70
				10	0.78	0.66	0.71	0.44	0.82	0.65
				20	0.76	0.70	0.67	0.52	0.75	0.70
			0.1	10	0.92	0.62	0.74	0.46	0.83	0.59
	0.3	0.7	0	5	0.87	0.48	0.90	0.38	1.10	0.33
				10	0.74	0.41	0.78	0.34	0.88	0.37
				20	0.60	0.41	0.61	0.35	0.67	0.43
			0.1	10	0.75	0.38	0.83	0.31	0.94	0.32
Mass Isolation	0.2	0.8	0	5	1.17	0.36	1.17	0.30	1.20	0.30
				10	0.91	0.28	0.93	0.25	0.94	0.30
				20	0.59	0.27	0.60	0.25	0.69	0.30
			0.1	10	0.91	0.26	0.92	0.21	1.07	0.29
Control Mass	0.2	0.3	0	5	0.84	0.85	0.78	0.64	0.86	0.77
				10	0.84	0.85	0.77	0.67	0.82	0.81
				20	0.90	0.89	0.79	0.75	0.88	0.86
			0.1	10	0.97	0.83	0.84	0.66	0.86	0.73

$$1.1 < m' < 1.2 , \qquad 0.2 < b < 0.4 \tag{15}$$

Moreover, it should be noted that as the point corresponding to the α_{s1} and α_{m1} values get closer to the upper left corner of the IRCS graph area, it is necessary to use larger practical damping value ξ_l of the link for more response reduction. To show the efficiency of the VSI in the case of long-period earthquakes (Group-2), in RSN165_IMPVALL earthquake sample, the corresponding IRCS graphs for viscous and visco-elastic links are shown

Table 7 Numerical results of the 5-story building with different isolation ratios subjected to selected earthquakes of Group-2

	α_{s1}	α_{m1}	β_l	$\xi_l(\%)$	RSN165_IMPVALL		RSN1231_CHICHI		RSN732_LOMAP	
					$R_{Flexible}$	R_{Stiff}	$R_{Flexible}$	R_{Stiff}	$R_{Flexible}$	R_{Stiff}
Interactional State	0.25	0.5	0	5	0.81	0.57	0.48	0.42	0.76	0.63
				10	0.68	0.56	0.53	0.49	0.65	0.63
				20	0.65	0.59	0.61	0.61	0.69	0.68
			0.1	10	0.73	0.50	0.62	0.41	0.76	0.57
	0.4	0.6	0	5	0.79	0.58	0.59	0.48	0.75	0.69
				10	0.72	0.57	0.63	0.58	0.70	0.70
				20	0.70	0.63	0.72	0.70	0.77	0.76
			0.1	10	0.75	0.50	0.72	0.51	0.81	0.66
	0.3	0.7	0	5	1.14	0.50	0.46	0.19	0.80	0.34
				10	0.92	0.40	0.42	0.23	0.70	0.40
				20	0.67	0.39	0.45	0.33	0.59	0.45
			0.1	10	0.92	0.35	0.49	0.21	0.76	0.34
Mass Isolation	0.2	0.8	0	5	1.31	0.28	0.59	0.09	1.29	0.17
				10	1.04	0.25	0.48	0.12	0.86	0.19
				20	0.70	0.27	0.37	0.17	0.57	0.26
			0.1	10	1.08	0.21	0.47	0.10	0.94	0.19
Control Mass	0.2	0.3	0	5	0.77	0.72	0.76	0.83	0.94	0.86
				10	0.79	0.78	0.84	0.86	0.83	0.89
				20	0.86	0.85	0.90	0.90	0.90	0.93
			0.1	10	0.87	0.77	0.94	0.81	0.94	0.86

in Figs. 20-21. Also, the corresponding statistical values are given in Table 4.

Based on the results presented in Figs. 20-21 and also Table 4, it can be seen that in the case of long-period earthquakes the general trend of optimal isolation ratios is almost the same. In case of viscous link, with an increase in the link damping value, the optimal coordinates move toward the upper left corner of the chart and in case of visco-elastic link, with an increase in the link stiffness value, no distinct trend of variation can be found for the optimal isolation coordinates. Nevertheless, in this case as well, Eq. (14) can be used as a tool for the preliminary design of the VIS.

8. Applying the VSI to a multi-Story building

To investigate the advantage of the VSI in low-rise multi-story buildings, the seismic performance of a 5-story building with the VIS was studied in comparison to an ordinary building of the same geometry. In this shear building model, the mass of stories was considered as 100 ton and their height as 3 meters. As described before, stories lateral stiffness values were selected in a manner that the maximum story drifts were limited to the seismic design code specified value. System inherent damping was assumed to be of Rayleigh type with 2% modal damping for the first and third modes of the original structure. It was also supposed that Rayleigh damping assumption remains valid for inherent damping characteristics of the individual VIS substructures. Dynamic characteristics of the 5-story building model are shown in Table 5.

Similar to the method employed in the 1-story model, estimation of the practical values of links damping in the multistory model was taken into account in terms of effective modal mass in the first mode of the structure. So, the upper limit practical modal damping value of about 20% of the original 5-story model was calculated as $c_{cr} = 2 M_1^* \omega_1$, and thus $c_{max} = 2 \times 417.74 \times 5.529 \times 0.2 = 923.87 (kN \, sec/m)$. The lower limit value of links damping was considered as $c_{min} = 2 \times 417.74 \times 5.529 \times 0.05 = 230.96 (kN \, sec/m)$ that corresponds to the damping ratio of 5% in the first mode of the original 5-story building. The damping values of the VIS interconnecting links were distributed uniformly in all stories. Considering the non-classical damping matrix of the VSI system, response history analyses were conducted by Runge-Kutta numerical method for different mass and stiffness ratios. The maximum inter-story drift in response history of each multi-story VIS and that of the original structure together were the basis for calculating response ratio and evaluation of the structural performance. Response ratios for earthquakes of Groups 1-2 in a moderate practical damping ratio of $\xi_l = 10\%$ are demonstrated in Fig. 22.

Based on these VICGs, it is observed that response ratios are satisfactory in the short multi-story buildings for both short-period and long-period earthquakes. This indicates that in multi-story buildings, in comparison to

one-story model, sensitivity to input earthquakes characteristics decreases because of the existence of different modes with different periods. Numerical results of the VSI in the 5-story model in some isolation ratios for selected earthquakes are given in Tables 6-7.

As it is seen in Tables 6-7, in assigning values to α_{s1} and α_{m1}, all states of the VIS, including interactional state (Eq. (14)), mass isolation as well control mass have been considered. Based on Table 6 and Table 7, it is understood that interactional states are more effective in response reduction since the response is controlled either via input energy dissipation in interconnecting link or by interactional actions. For mass isolation state ($\alpha_{s1} = 0.2$, $\alpha_{m1} = 0.8$) as discussed earlier, it is inevitable to use larger values of damping to have satisfactory response control. Finally, the specific cases of the VSI in which mass and stiffness ratios of flexible substructure are assigned intentionally in such a way that its mass is smaller considerably than stiff substructure (areas at the left lower corner of TUT in the VICG shown in Fig. 22). This condition can be interpreted as the control mass state and this is one of the convenient approaches in the VSI. The control mass state is numerically recognized with isolation ratios as $\alpha_{s1} = 0.2, \alpha_{m1} = 0.3$ in Tables 6-7. One of the features of this state is that using visco-elastic links with moderate damping values could be effective in response reduction as it is usual in using TMD.

9. Conclusions

In using the VSI technique in a building, a variety of strategies can be considered. These strategies must be selected according to architectural design, building occupation, the original structural configuration, constructional costs and especially the link type and values of reachable added damping in energy dissipation devices. The results of numerous analyses on different earthquakes excitation, performed in this study, imply that employing appropriate link parameters proportional to mass and stiffness ratios can lead to satisfactory levels of seismic response reduction. However, according to mass and stiffness ratios, three different states can be differentiated. Using control mass and mass isolation which are two extreme states and also the intermediate VSI which is interactional state leads to seismic response reduction in both of substructures. On this basis, the following remarks can be stated as the conclusions of this study

• By applying the VSI technique to low-rise multi-story buildings, in interactional state, using the proposed relationship between α_{s1} and α_{m1} (given by Eq. (14)) with the suggested ranges of parameters, up to 50% decrease in the seismic response of flexible substructure and even more in stiff substructure is achievable. In this state, it is practical to select a wide variety of mass and stiffness ratios with different link damping values. However, using larger values of link damping, the sensitivity of isolation ratios to input earthquakes characteristics decreases, therefore, the system behaves

in a more reliable manner.
• In mass isolation state of the VSI, major portions of the building's mass and stiffness are assigned individually to each of the substructures. The suggested ranges of isolation ratios in this state are $\alpha_{m1} \geq 0.8$ and $\alpha_{s1} \leq 0.2$, which are limited ranges. To achieve the reliable response reduction in this state, it is inevitable to use relatively large values of practical link damping as 15 to 20%.
• Increasing the link damping in the practical range generally leads to seismic response reduction in both substructures of the VIS; nonetheless, flexible substructure response is more dependent on link damping value than the stiff one.
• Link stiffness in the practical range less than 10% of the original structure does not affect response reduction of flexible substructure, while it can make stiff structure behave more satisfactorily.
• The values of inter-story drifts in low-rise multi-story VSI buildings are less sensitive to input earthquakes characteristics (short and long-period earthquakes) as well as isolation ratios, comparing to the 1-story frame.

Finally, it should be noted that the present study was limited to linear dampers. To extend the results to more general cases, such as nonlinear dampers, further research is necessary.

Acknowledgments

References

Abdeddaim, M., A. Ounis, N. Djedoui and M. Shrimali (2016), "Pounding hazard mitigation between adjacent planar buildings using coupling strategy", *J. Civ. Struct. Hlth. Monit.*, **6**(3), 603-617.

Abdeddaim, M., A. Ounis, N. Djedoui and M. Shrimali (2016), "Reduction of pounding between buildings using fuzzy controller", *Asian J. Civ. Eng.* (BHRC), **17**(7), 985-1005.

Bharti, S., S. Dumne and M. Shrimali (2010), "Seismic response analysis of adjacent buildings connected with MR dampers", *Eng. Struct.*, **32**(8), 2122-2133.

Dumne, S., M. Shrimali and S. Bharti (2017), "Earthquake performance of hybrid controls for coupled buildings with mr dampers and sliding base isolation", *Asian J. Civ. Eng.* (BHRC), **18**(1), 63-97.

Klein, R., A. Todaro and I. Finne (1972), "Investigation of a method to stabilize wind induced oscillations in large structures", *Am. Soc. Mech. Engineers*, **95**(2), 53-53.

Lee, D. and D.P. Taylor (2001), "Viscous damper development and future trends", *Struct. Des. Tall Build.*, **10**(5), 311-320.

Nekooei, M. and M. Ziyaeifar (2008), "Spectral investigation on the seismic behaviour of vertical mass isolated structures against Earthquake", *The 14th World Conference on Earthquake Engineering*.

Nekooei, M. and M. Ziyaeifar (2008), "Vertical seismic isolation of structures", *J. Appl. Sci.*, **8**(24), 4656-4661.

Nigdeli, S.M. and G. Bekdas (2014), "Optimum tuned mass damper approaches for adjacent structures", *Earthq. Struct.*, **7**(6), 1071-1091.

Patel, C. and R. Jangid (2010), "Seismic response of dynamically similar adjacent structures connected with viscous dampers", *The IES Journal Part A: Civil & Structural Engineering*, **3**(1), 1-13.

Richardson, A., K.K. Walsh and M.M. Abdullah (2013), "Closed-form equations for coupling linear structures using stiffness and damping elements", *Struct. Control Hlth. Monit.*, **20**(3), 259-281.

Xu, Y., Q. He and J. Ko (1999), "Dynamic response of damper-connected adjacent buildings under earthquake excitation", *Eng. Struct.*, **21**(2), 135-148.

Zhang, W. and Y. Xu (1999), "Dynamic characteristics and seismic response of adjacent buildings linked by discrete dampers", *Earthq. Eng. Struct. D.*, **28**(10), 1163-1185.

Zhang, W. and Y. Xu (2000), "Vibration analysis of two buildings linked by Maxwell model-defined fluid dampers", *J. Sound Vib.*, **233**(5), 775-796.

Zhu, H., D. Ge and X. Huang (2011), "Optimum connecting dampers to reduce the seismic responses of parallel structures", *J. Sound Vib.*, **330**(9), 1931-1949.

Zhu, H. and Y. Xu (2005), "Optimum parameters of Maxwell model-defined dampers used to link adjacent structures", *J. Sound Vib.*, **279**(1), 253-274.

Ziyaeifar, M. (2000), "Method of mass isolation in seismic design of structures", *Proceeding of the 12th World Conference on Earthquake Engineering*, Paper.

Ziyaeifar, M., S. Gidfar and M. Nekooei (2012), "A model for mass isolation study in seismic design of structures", *Struct. Control Hlth. Monit.*, **19**(6), 627-645.

CC